Shadowgraph Optical Technique for Measuring The Shock Hugoniot From Standard Electric Detonators

Vilem Petr. Research Associate Professor and Technical Director of AXPRO Group, Colorado School of Mines, 1600 Illinois Street, room 120, 80401, Golden, CO.

Erika Nieczkoski. Research Assistant at AXPRO Group, Colorado School of Mines, 1600 Illinois Street, room 129, 80401, Golden, CO.

Eduardo Lozano. Research & Teaching Assistant at AXPRO Group, Colorado School of Mines, 1600 Illinois Street, room 129, 80401, Golden, CO.

Abstract

This research paper overviews the detonation characteristics of the liquid-desensitized function detonator used for the oil and gas industry. The liquid-desensitized function is designed to protect perforating tools from any liquid that penetrates inside the tool during operation. Additionally, the number eight standard electric detonator is analyzed using the same technique. The measurement of the energy release from these types of initiation systems becomes critical for the evaluation of their initiation ability of the firing sequence, as well as from the standardization point of view.

The Advanced Explosive Research Processing Group (AXPRO) presents a new method for experimentally measuring air shock properties and energy fluence from detonators by the using a single indoor experiment. The retro-reflective shadowgraph technique was used for measuring shock wave expansion rate. The method was effectively improved by replacing the continuous light with a strobe light. This new technique allows us to obtain much higher image quality than the one obtained by the Schlieren method. The shock Hugoniot and conservation equations provided a full characterization of the released energy from the high explosive base charge contained within the detonator. This technique produces data in general agreement with published data for the detonation and air shock properties from high explosives. This new method could constitute a practical and simplified experimental tool for industry use due to its relatively low cost, high data accuracy, and reduced data-analysis time.

Keywords: high-speed imaging, retro-reflective, shock wave, detonation, and initiation system.

1. Introduction

In order to initiate high explosives and the blasting agents, strong shock or detonation is required. A capsule of sensitive explosive material termed a detonator can accomplish this. Figure 1 shows two different designs of electric detonators that are generally used throughout the world. One is a standard

mining and construction detonator Electric SP Number 8 and the other is a fluid desensitized oil and gas detonator Number 6.

High-speed imaging technologies are constantly being improved for the study of detonation properties of explosive materials [1-9]. The goal of this research was to develop a "relatively simple" experimental method that validates the explosive energy inside of a detonator. The challenge of this endeavor emerges from the nature of manufacturing; detonator designs are always unique and the composition, as well as the combination, of explosive materials used is variable and depends on the manufacturer.

The first detonator was developed in 1890s, and had a single explosive base. Since then, there have been significant improvements in initiation system technology. Presently, detonators frequently have two different explosive base materials: a sensitive primary explosive (primer charge), and a less sensitive, but more high-powered (brisance) secondary explosive (base charge), as is shown in Figure 1.

Detonator technology has developed significantly since the first initiation system was created. In general, a detonator consists of a metal capsule, tube or shell. The first detonator shells were constructed from paper, and then later advanced to copper, bronze, aluminum, and finally, plastic in the pursuit of the mitigation of fragments. There have also been advancements to universal detonator requirements. The United Nations' specifications for electric detonators generally require a 7.00 to 8.00 millimeter diameter and a varying length depending upon whether the detonator is an instantaneous or delay type.

When manufactured, the detonator base charge is placed at the bottom of the metal shell. Both the primer charge and the base charge are compacted together under adequate pressure to ensure the desired strength. Strength of detonator is based upon the quantity of base charge and primary charge; detonators are typically numbered from their strength. Traditionally, detonator strength is characterized through manual indirect measurement techniques. These techniques require detonating an initiation system into a soft medium (Sand Test, 1916), or in some cases, next to a lead or/and metal witness plate (plate test), are time consuming and imprecise. On other hand high-speed imaging systems, which were previously unfeasible for research and development use due to their high-expense, are now an obvious replacement for these methods.

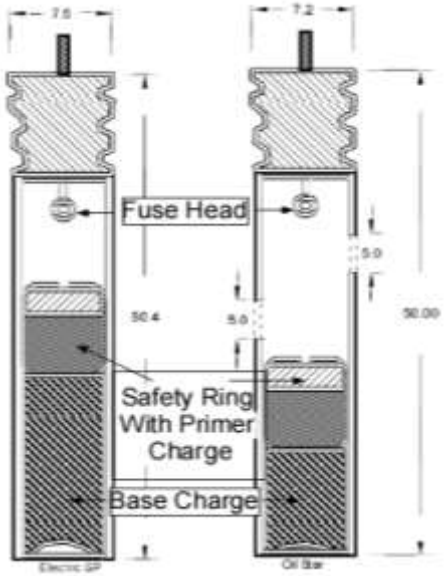

Figure 1. Two main electric detonators types used in mining and construction and oil and gas industries. Units are in millimeters.

2. Theory Background

A high explosive material is characterized by a detonation process where the front of the chemical reaction moves faster through the material than its speed of sound. This sudden release of energy is usually accompanied by the creation of a propagating disturbance in the surrounding medium known as shock or blast wave. By knowing the medium and the rate of expansion of this shock wave, one is able to characterize not only the shock effects on the medium, but also the energy source.

The shock front of a blast wave is in many ways a determining factor in its behavior. The goal of this paper is to characterize detonator initiation strength from its performance in air, which for present purposes may be considered as an ideal gas. Using a Lagrangian coordinate system one can describe the five basic parameters in the air before and after the pass of the shock front. Three first relationships can be derived from the fact that we must conserve mass, momentum, and energy across the shock front. At this point, an equation describing the equilibrium states in which a material can exist in expressed by the Equation of State (EOS). This equation was empirically determined by many experiments in the past, and it was found that the shock velocity was linearly related to the particle velocity for most materials [10]. This empirical relationship is called Hugoniot and it is expressed as follows:

$$U = C_0 + su$$

Where U represents shock velocity, u is particle velocity, C_0 is bulk sound speed, and s is a dimensionless term. For air, Deal (1957) measured Hugoniot coefficient C to be 2,375 m/s and s to be 1.0575 for measured shock wave velocities up to 4,500 m/s. As reported by Biss (2013), using these equations, it is possible to calculate the transmitted shock wave properties in air through the sole measurement of the air shock wave expansion rate. From the measure of the detonator shock wave expansion rate in air, the incident air shock wave properties are determined: shock wave velocity U_s, shock wave Mach number M_s, particle velocity u_s, and incident shock wave pressure P_s. Additionally, the energy per unit area or energy fluence transferred from the detonator to an another possible energetic material can be calculated from the values of shock wave pressure P_s, and time duration t_d if the properties (Hugoniot) of the material are known.

3.1 Air Shock Characterization

The present paper reports the shock wave expansion from two types of electric detonators corresponding to two different values of strength: number six and number eight. The expansion is measured in two coordinates X and Y, corresponding with the longitudinal and transversal axes of the detonator. This is due to the initial elliptical expansion of the shock wave in the 2D plane produced by the charge geometry. As the shock wave expands, it decays in strength, lengthens in duration, and slows down, both because of the spatial divergence and because of the medium attenuation.

Most of the sources of compiled data for air blast waves from high explosives are limited to bare, spherical charges in free air. However, different experiments conducted with alternative charge geometries show how explosive materials tens to drive their energy to the larger area of their outer surface. Esparza (1992) presented a spherical equivalency of cylindrical charges in free air where a higher explosive yield is reached at 90 degrees from the longitudinal charge axis. The difference in the shock wave magnitude in the different directions will decrease as the shock expands through the air adopting a final spherical shape. This data is in agreement with the experimental observations presented

in this paper where the two detonator studied are cylindrical in shape. This shape will produce an initially ellipsoidal expanding shock wave creating higher overpressure in the plane normal to the charge axis. As the shock wave moves outward, the initial ellipsoid will degenerate into an expanding sphere.

The shock wave expansion rate in atmospheric air is experimentally measured by using a retro-reflective shadowgraph technique. This expansion is measured along the longitudinal and transversal axes of the detonator providing two set of data. The measured shock wave expansion rate is then fitted to an empirical equation developed by Dewey (1964) and reported by Hargather et al. (2008) and Biss (2009). This empirical correlation is as follows:

$$R_s(t_a) = A + Ba_0t_a + Cln(1 + a_0t_a) + D\sqrt{ln(1 + a_0t_a)} \quad (1)$$

Where R_s represents distance from the center of the blast, t_a represents time of arrival of the shock wave, a_0 is the local speed of sound, and A, B, C, and D are the yielding coefficients. For curve fits to data close to the charge center, B should be set to 1 to guarantee an asymptote to the speed of sound for large time [14]. The calculation of the parameters A, B, C, and D was performed by least-squares curve-fit through a computational code written in MATLAB [15].

Next, a relationship between shock velocities versus time can be obtained by simple derivation of the Equation (1) for longitudinal and transversal directions:

$$\frac{dR_s(t_s)}{dt_s} = Ba_0 + \frac{Ca_0}{1 + a_0t_s} + \frac{Da_0}{2(1 + a_0t_s)\sqrt{ln(1 + a_0t_s)}} \quad (2)$$

An explosive shock moving with a certain velocity U_s into an atmosphere where the sonic or acoustic speed is C_a will produce an associated pressure jump known as overpressure of the explosive shock front. Assuming a constant heat capacity ratio for air of 1.4, Kinney and Graham (1985) defined the following equation describing the blast overpressure as a function of the shock Mach number $M_s=U_s/C_a$ and the atmospheric pressure P_a.

$$P_s = \frac{7({M_s}^2 - 1)}{6} \cdot P_a \quad (3)$$

As can be deduced from Equation (3), for shock waves generated in an explosion, where intensity of shock diminishes with distance from the center of the explosion, shock overpressure approached zero and shock velocity approached sonic as distance increases. That is, any explosive shock wave ultimately degenerates into a sound wave. Equation (3) and some alternative forms presented in reference [17] have been widely used for indirect computation of overpressures from shock velocity measurements.

In order to fully characterize the explosive energy release, the duration of the overpressure must be calculated. Kinney and Graham (1985) proposed a theoretical method for the calculation of the positive phase duration upon knowing the speed of the shock wave as a function of the radius and assuming that the point marking the end of the positive pressure phase travels at the speed of sound of the gas right behind the shock wave. This blast overpressure duration can be calculated from the shock Mach number versus the distance by the Rankine-Hugoniot theory where each point is assumed to have a static temperature caused by a shock wave passing at a given Mach number [17].

Ultimately, in order to validate overpressure-duration values indirectly calculated from the optical methods presented in this paper, pressure sensors recorded direct measurements of blast overpressure from the passage of the shock wave.

3.2 Initiation Strength: Energy Fluence

A detonator is a device used to trigger by shock an explosive device. The energy released by this shock becomes essential while determining the strength of such detonator. Experiments have been conducted in the last decades using different initiators such a flyer plates, where the shock pressure was varied by changing the impact velocity. Each explosive was found to have a unique range of energy fluence above which prompt detonation was always obtained, and below which it was not. The average of this range is called the "critical energy fluence"[10]. For this reason, the energy provided by the detonator must be accurately calculated in order to evaluate its initiation ability assuming not only a direct contact charge-detonator, but also in the case of a certain standoff distance (Gap Test). The term energy per unit area or energy fluence is then expressed as follows:

$$E = \int P u_p dt \approx \frac{P^2 t_d}{2\rho_0 U} = \frac{P^2 t_d}{2Z_{material}} \tag{4}$$

Where the P is the shock pressure, t_d is the shock duration, ρ_0 is the density of the material and U is the shock velocity on the material (detonation velocity for high explosives). The denominator is often called the shock impedance of a material and for the range of overpressure involved in shock initiation, it can be considered to be nearly constant for each explosive [10]. It should be noted, that the energy fluence will be dependent on the energy source and the matter where the energy is transferred. Equation (4) represents a rough approximation of the integral because the profile of the blast overpressure versus time will change with the time producing different wave form factors. For the purpose of this paper and in order to provide a simple solution, the shock wave profile is assumed triangular which adds a factor of 2 in the divider.

Different approaches have been unsuccessfully addressed for the measure of the energy release from optical methods. The classical similarity solution for a point energy release and strong shock wave formation by Taylor predicts the motion of the shock wave and the resulting physical property distributions and using the dimensional analysis [19]. This ideal prediction however cannot be directly applied to typical explosions where the energy is released over a finite time. These real explosions are better analyzed experimentally by measuring shock propagation or property variations then applying scaling laws [15]. Here, the shock propagation is measured from the center of the explosive as a function of time and becomes the primary data for developing an explosive characterization.

4. Experimental Procedure

4.1.1 Number #6: detonator with fluid-desensitizing function and Number #8: Electric SP

Based upon the quantity of base and A.S.A charge, detonators are designated from No.1 to No.10, with the standard detonator being the Number 8 detonator. From design alone, we should expect to see the Number 8 detonator produce a much stronger pressure pulse than a Number 6 detonator, as the Number 8 contains 0.35 grams of A.S.A mixture and 0.25 grams of base charge.

Table I, below, showing the first detonators specifications for only the base charge (mercury fulminate),

was the first classification for blasting cups according the blasting strength, and still used today. In general, a Number 8 classic detonator can be described as a metal shell that contains a secondary base charge (typically PETN, RDX, HMX) which is capped with a primary charge (typically mercury fulminate, lead azide, or silver fulminate), positioned on one end of the shell. Adjacent to this, but a sufficient distance away, is a fuse head, a low donor explosive, embedded with a bridge wire, which connects two leg wires, thus forming a means of electrical ignition. If a firing current is applied to the leg wires, the bridge wire becomes incandescent, and the fuse head is initiated. This initiation has enough force to initiate the very sensitive primary charge, and subsequently the secondary charge.

The Number 6 fluid-desensitized detonator is quite similar to the Number 8 detonator. However, as it is used in the oil and gas industry for perforating guns, it operates in a very specific manner. Because the detonator is often exposed to a wet environment, RDX, which is water-resistant, is the strictly used secondary explosive. To prevent industrial accidents and expenses from the accidental leakage of water into a perforator, the Number 6 fluid desensitized detonator is manufactured with two holes between the fuse head and the primary and secondary explosive cap. Should any liquid fill the space between fuse head and the charges, then the initiation of the fuse head charge should not have enough force to initiate the explosives (at a sufficient amount of pressure due to depth in the liquid).

Table I. Different amount of lead azide explosives to characterize the strength of detonator.

Detonator Standard No.	1	2	3	4	5	6	7	8	9	10
Mercury Fulminate (grams)	0.3	0.4	0.54	0.65	0.8	1	1.5	2	2.5	3

4.2 Shadowgraph Technique

Shadowgraphy was invented as a visualization method in 1672, where the Sun was used to cast a shadow on a white surface. “Modern” shadowgraphy differs from this more rustic method in its use of specialized screens, light sources, and high-speed imaging systems.

The direct shadowgraph technique is simple and robust, requiring only a light source, a camera, and a screen on which to cast a shadow. In general, a light source is placed at an optimum distance, *L*, from the screen, and from refractive disturbances in the Schlieren object, a shadow is projected at a certain height, *h,* onto the screen. Edgerton retro-reflective shadowgraphy, specifically, requires the use of a retro-reflective screen and a rod mirror, which is aligned with the camera axis, illuminating the retro-reflective screen with a significant amount of light, and thus providing a high quality image. This technique is useful for the characterization of explosive energy, as it is able to measure blast wave parameters in the air, while also “de-emphasizing other, less abrupt flow features” [1]. According to United Nations’ specifications, a detonator must have a reaction within 25 microseconds, and must deliver a detonation velocity of 8,000 meters per second – undoubtedly, the Edgerton retro-reflective shadowgraph technique would be very useful for manufacturers or explosive users who are looking to control and understand the specifications of their product or purchase. In order to explore the shockwaves generated by laboratory-scale explosions from the two categories of detonator, a combination of modern high-speed videography and Edgerton shadowgraph was used.

4.2.1 Retro-reflective Shadowgraphy Experimental Methods

The experimental setup used during the experiments is shown in the image below. High speed camera, collimated strop lighting system, lens with rod mirror, and a retro-reflective screen are required instrumentation for the execution of Edgerton shadowgraph.

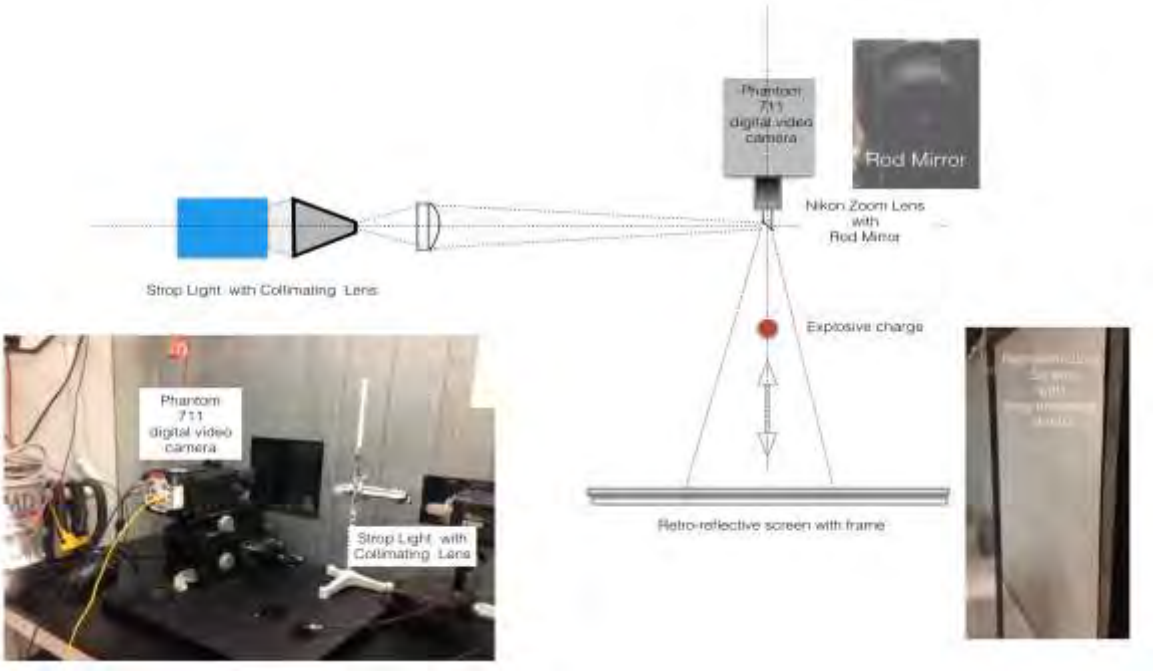

Figure 2. Edgerton retro-reflective shadowgraph system, top view

Our Edgerton shadowgraph setup, shown in Figure 2, is elegant in its simplicity, robustness, and ease of use. The system is most appealing for small-scale blast chamber applications, as it consists only of a retro-reflective screen, a rod mirror, a high-speed imaging system, and a light source.

The retro-reflective screen is made of 3M Scotchlite TM 7610, a high gain, industrial grade, exposed-lens, plastic-based material pre-coated with a pressure-sensitive adhesive. An industrial supplier can provide screens made of this material. Our currently used screen is a 2.4 meter square and costs about 4000 USD.

4.3 Pressure Gauges

Two PCB Piezotronics model 137A23 pressure gauges are placed in the camera plane for the validation of the shock wave incident pressure and positive time duration. Both sensors were mounted in a steel rod pointing in an axial direction to the detonator. Standoff distances from the energy source varied from 325 mm to 430 mm. At that range, and considering the explosive yield within the detonator, the sensitivity of the pressure sensors seems reasonable (100 mV/psi). The diaphragm was insulated using common black vinyl electrical tape to minimize possible signals generated by flash temperatures due to the passing of the shock front. Additionally, the bodies of the gauges were isolated from the ground by placing common black vinyl electrical tape in the contact surface with the steel rod.

The two pressure sensors were connected by coaxial cable to a PCB sensor signal conditioner model 482C05. Both outputs were also connected to channel 1 and channel 2 of a Tektronix DP 3014 Oscilloscope where the signal provided by each gauge was recorded. Triggering was implemented from

the firing machine and a signal differentiator which provides with a 2 volts output to the lighting system, high-speed camera, and Oscilloscope.

5. Results and Discussion

5.1 Camera results

The events were captured by using a Phantom High Speed Camera v.711. Resolution of the image was set to 912x848 with a sample rate of 9100 fps, and 0.294us exposure. Frame sequences for Number 6 and Number 8 detonators are shown in Figure 4. The shock wave front traveling outwards has been highlighted with a white contour. As it is shown, the initial blast wave presents a sharp elliptical shape due to charge geometry. As the shock expands, the patial divergence and medium attenuation cause a gradual change in shape ending as a spherical shock wave (frame 7). Thirty Number 6 electric detonators and fifty Number 8 detonators were tested by the use of this technique. This technical paper only reports the results obtained for one test per detonator as demonstration of the technique.

The ellipsoidal shock generated by the explosive charge produces higher shock velocity values in the transversal plane of the charge versus those recorded in the longitudinal axis. For this reason, the explosive energy delivered by the detonator will be different for each direction with respect its body. This difference will decrease as one moves away from the center of the explosion as it will show in the following sections. The next diagram illustrate the two dimensional position of each axis with respect to the body of the detonator.

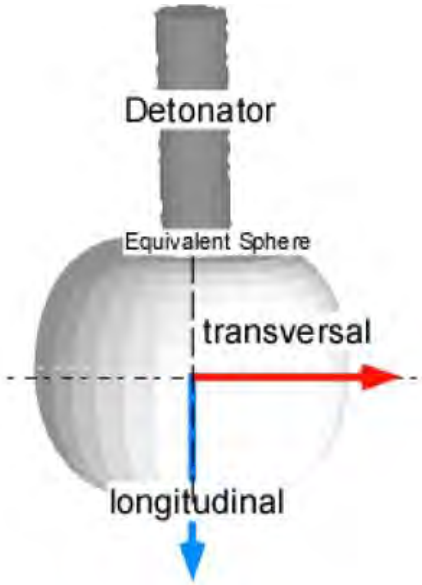

Figure 3. Axis position with respect to the detonator's body and base charge's location

Additionally, the symmetry axis of a cylindrical detonator corresponds with its longitudinal axis and therefore seems reasonable to assume that the shock expansion in the normal plane of the camera view will be equal to the one recorded along the transversal direction. In order to accurately measure this third dimension, a second high speed camera would be required.

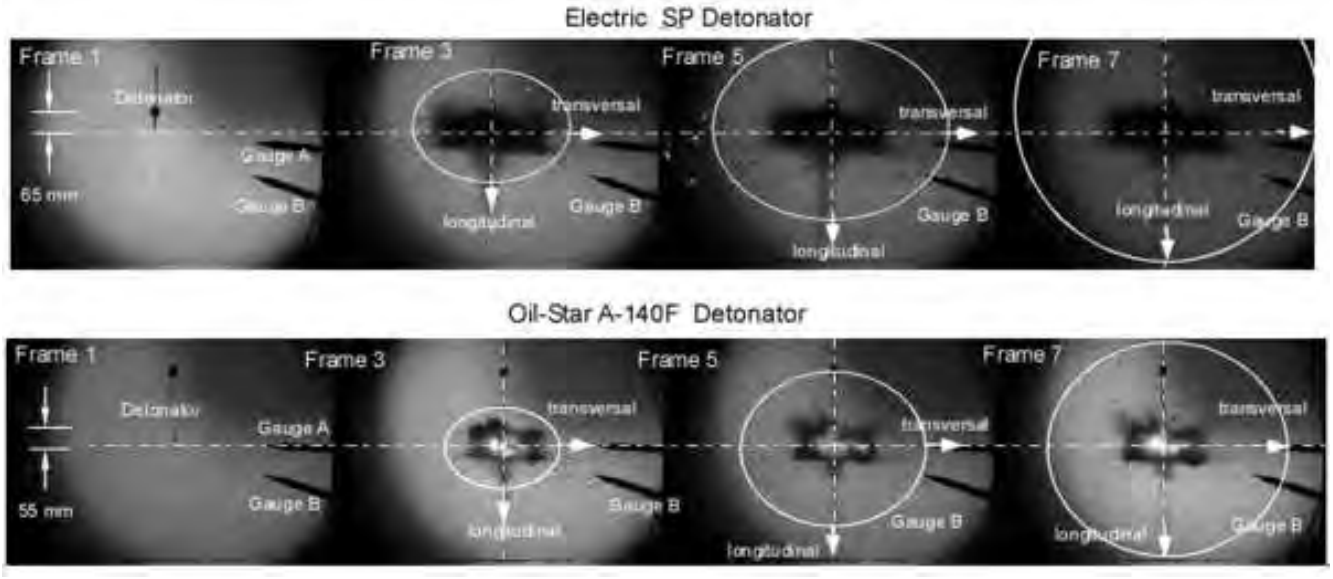

Figure 4. Frame sequence for electric detonator #8 (top) and #6 (bottom)

5.2 Gauge measurements

For the Number 8 electric detonator, gauges A and B were placed in the plane of the camera and at a distance of 325 mm and 345 mm from the center of the explosion. Gauge A was place approximately aligned with the transversal axis of the detonator (-4˚ from the transversal axis) and Gauge B at -20˚ from the transversal axis.

A triggering delay was measured from the actual triggering to the instant of initiation in the detonator. This triggering delay was calculated using the frames of the camera because of its almost instant response and the very short length of the cables employed. From t_0 to the actual instant of the detonation, a triggering delay of 400 us was measured and subtracted in the oscilloscope triggering signal during the experiment by using a delay generator. The sample length was 10,000 with a sample rate set to 500 KS/s. The next two Figures show the signal recorded from Gauges A and B from the initiation of the detonation. P_s represents peak incident overpressure, t_a is the time of arrival of the shock, and t_d is the measured positive phase duration.

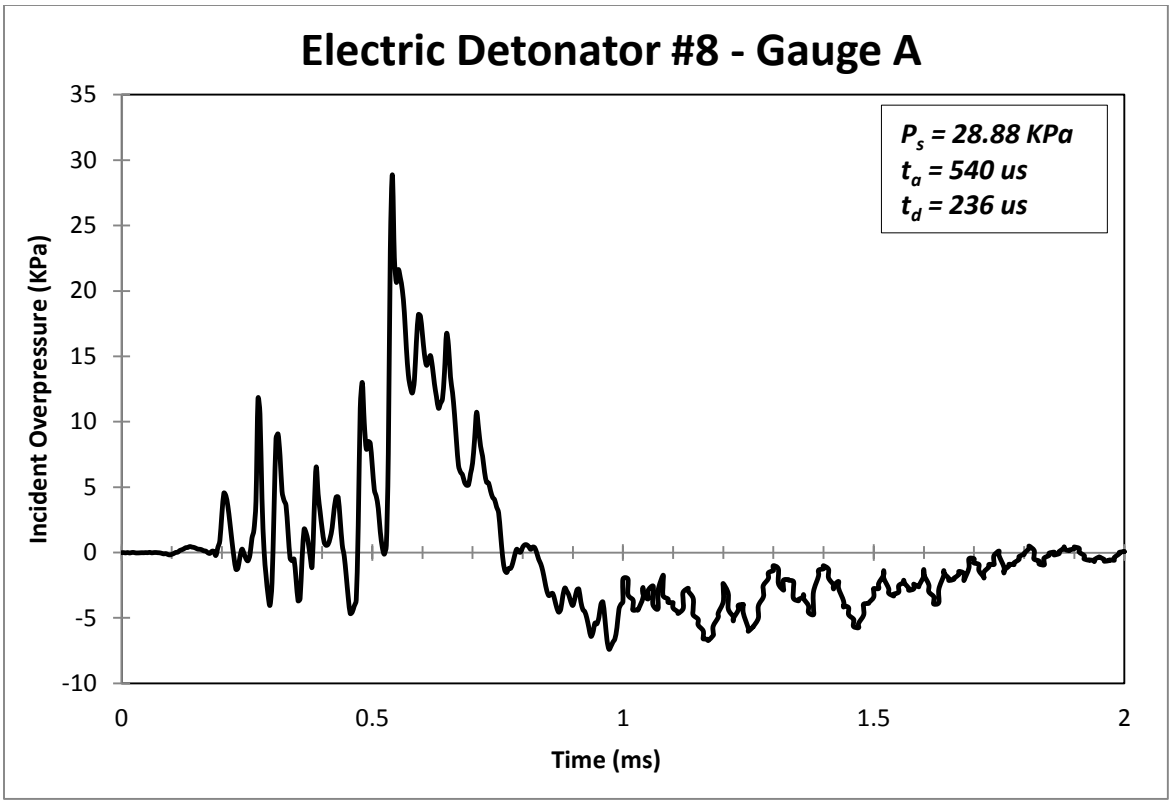

Figure 5. Incident overpressure versus time. Detonator #8 Gauge A. Standoff: 325 mm. Angle: -4˚

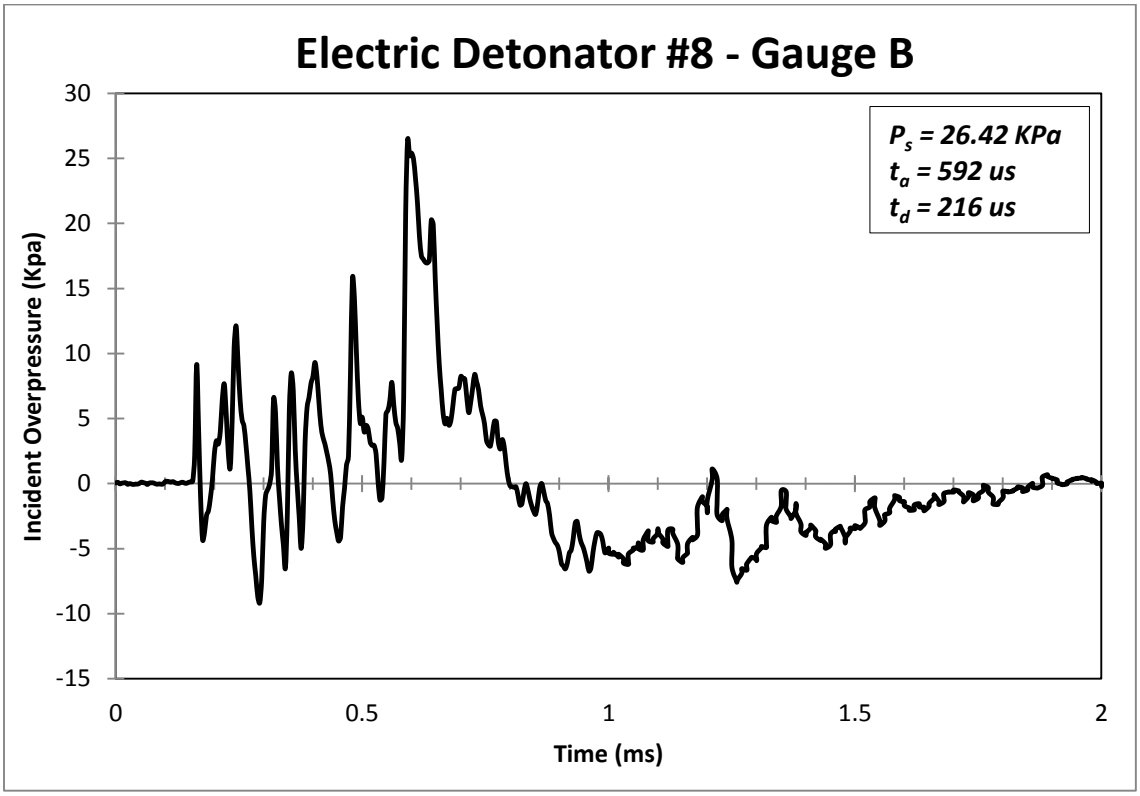

Figure 6. Incident overpressure versus time. Detonator #6. Standoff: 345 mm. Angle: -20˚

As it is shown in Figures 5 and 6, the gauge located in the transversal axis recorded a higher peak incident overpressure. This fact corresponds with the images obtained by the shadowgraph where the higher shock velocities are produced throughout this axis.

The gauge lectures are also noised during a certain period of time before the shock arrival. By observing the images provided by the high speed camera, the experimentalist can deduce that the peaks generated are due to the Mach waves produced by the primary fragments from the detonator aluminum casing during their supersonic flight.

A similar analysis is performed for the number 6 electric detonator. Gauges A and B were placed in the plane of the camera and at a distance of 410 mm and 430 mm from the center of the explosion. Gauge A was place approximately aligned with the transversal axis of the detonator (+2˚ from the transversal axis) and Gauge B at -15˚ from the transversal axis.

The same triggering delay of 400 us was measured and subtracted in the oscilloscope triggering signal during the experiment by using a delay generator. In this case the sample length was 100,000 with a sample rate set to 5 MS/s. The next two Figures show the signal recorded from Gauges A and B from the initiation of the detonation. P_s represents peak incident overpressure, t_a is the time of arrival of the shock, and t_d is the measured positive phase duration.

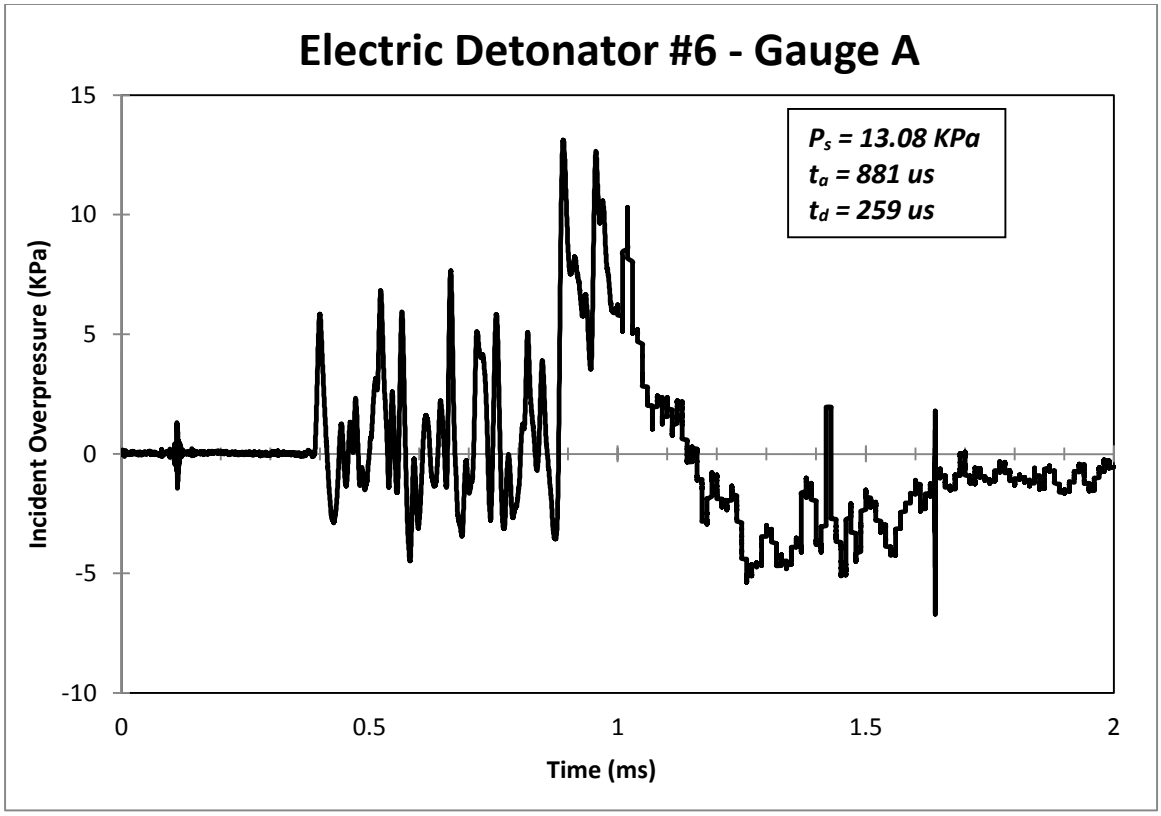

Figure 7. Incident overpressure versus time. Detonator #6 Gauge A. Standoff: 410 mm. Angle: +2˚

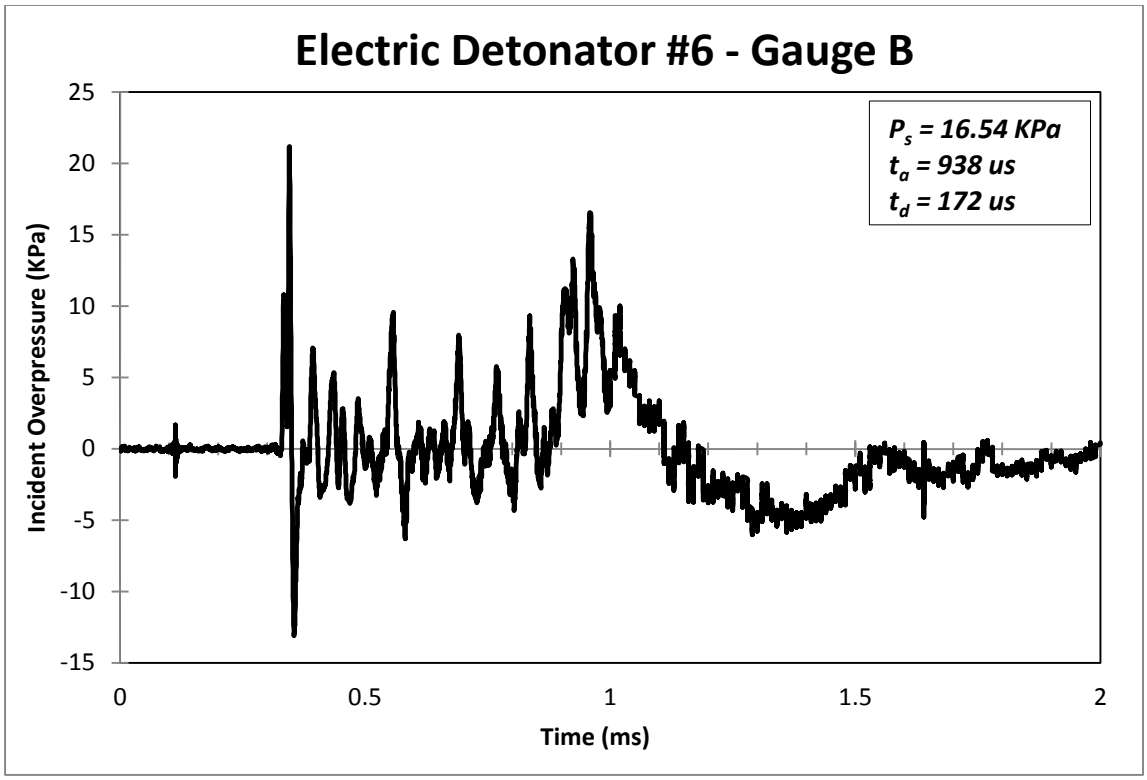

Figure 8. Incident overpressure versus time. Detonator #6 Gauge A. Standoff: 430 mm. Angle: -15˚

As it is shown in Figures 7 and 8, the gauge located in the transversal axis recorded in this case a lower value of overpressure. One possible explanation is the unintentional error induced in the pencil gauge tilting producing a lower value than expected because of the oblique shock interaction. For this detonator, the gauge lectures are also noised during a certain period of time before the shock arrival due to the Mach waves generated by the supersonic fragments initially traveling at a higher speed than the blast shock front.

Two verifications are recommended in order to check a good data collection while using pressure sensors. First, a rising time less than 10us from the zero line to 2/3 of the maximum incident overpressure pulse is recommended in order to validate a proper sensor's response. Second, adequate pressure sensor sensitivity can be confirmed by a signal to noise ratio less than 10. In other words, when dividing the maximum peak overpressure (voltage) recorded by the peak to peak noise value, the result must be always less than 10. A lower ratio value would be symptom of too low gauge sensitivity for the desired experiment. In this case, for each of the four measurements performed by the pressure gauges, these two conditions are ample satisfied.

Relating to data interpretation, two other considerations are recommended to take into account. The maximum value recorded by the oscilloscope will not exactly match with the peak incident overpressure because of the resolution of the oscilloscope. Oscilloscopes with low resolution (low number of bits) will approximate to a larger voltage level during the measurements. For our purposes, we can consider the difference negligible. If a higher accuracy is desired, a good method for obtaining a closer value to the real peak overpressure is by the fitting of the waveform. A second consideration in data analysis is that pressure sensors tend to keep a higher temperature after the passing of the positive blast pulse, ending with larger "P zero" values than in the real experiment. This fact might imply relatively low impulse measurements.

5.3 Air shock properties and Energy Fluence

Three different tests are reported in this technical paper. Due to camera resolution and sample rate, 8 to 9 points are recorded from the instant of the detonation, each of them corresponding with a camera frame. From the images, the shock wave expansion in each direction within a 2D plane is successfully measured. For the purpose of this document, two directions are recorded corresponding with the longitudinal and transversal axis of the detonator. The same behavior observed for the transversal direction is assumed for the third dimension due to charge symmetry. Therefore two measurements are implemented from the high-speed images provided by the camera: shock wave expansion rate in the transversal direction and shock wave expansion rate in the longitudinal direction. Additionally, by assuming than the volume of air being compressed by the ellipsoidal shock wave is the same than the one compressed by an equivalent sphere of radius *R*, one can provide an estimation of the expansion rate for an equivalent spherical shock wave. For explosive yield determination, this assumption seems convenient since most of the data from high explosives is expressed for spherical blast waves. It must be remarked than this initial ellipsoidal blast wave will end up adopting a spherical shape due to geometrical expansion and medium attenuation.

From the camera frames, the shock wave distance versus time from the center of the charge is collected for the two models of electric detonators. By applying least-squares regression, coefficients *A, B, C* and **D** are determined for the use of the Dewey's Equation. The coefficients are determined 6 different times, one for each shock wave propagation direction (transversal, longitudinal, and spherical equivalent) and per detonator (Number #8 and Number #6). The next table summarizes the calculated parameters values along with the coefficient of determination per curve.

Table II. Curve fitting coefficients for Dewey's Equation

Detonator	Direction	A	B	C	D	R^2(%)
#6	Transversal	3.3606	1	28.8071	-20.8846	99.90%
	Longitudinal	3.4813	1	38.9471	-62.4522	99.99%
	Spherical Equ.	3.4017	1	34.0745	-39.4129	99.95%
#8	Transversal	3.5594	1	25.4924	2.0478	99.95%
	Longitudinal	3.737	1	43.593	-56.1228	99.88%
	Spherical Equ.	3.6229	1	33.0109	-21.0115	99.99%

The next two figures represent the shock wave expansion rates (data points and fitting curves) for Number 6 and Number 8 detonators in transversal and longitudinal directions. Additionally, the expansion rate of an equivalent spherical wave is plotted.

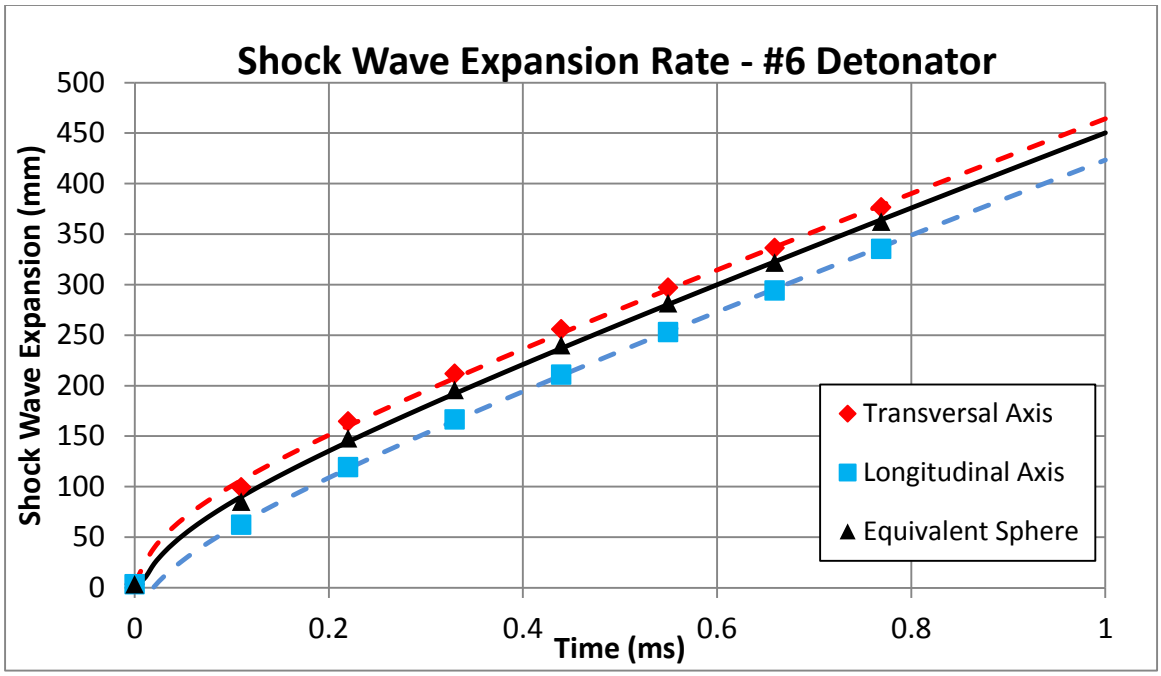

Figure 9. Shock wave expansion rate for number #6 electric detonator

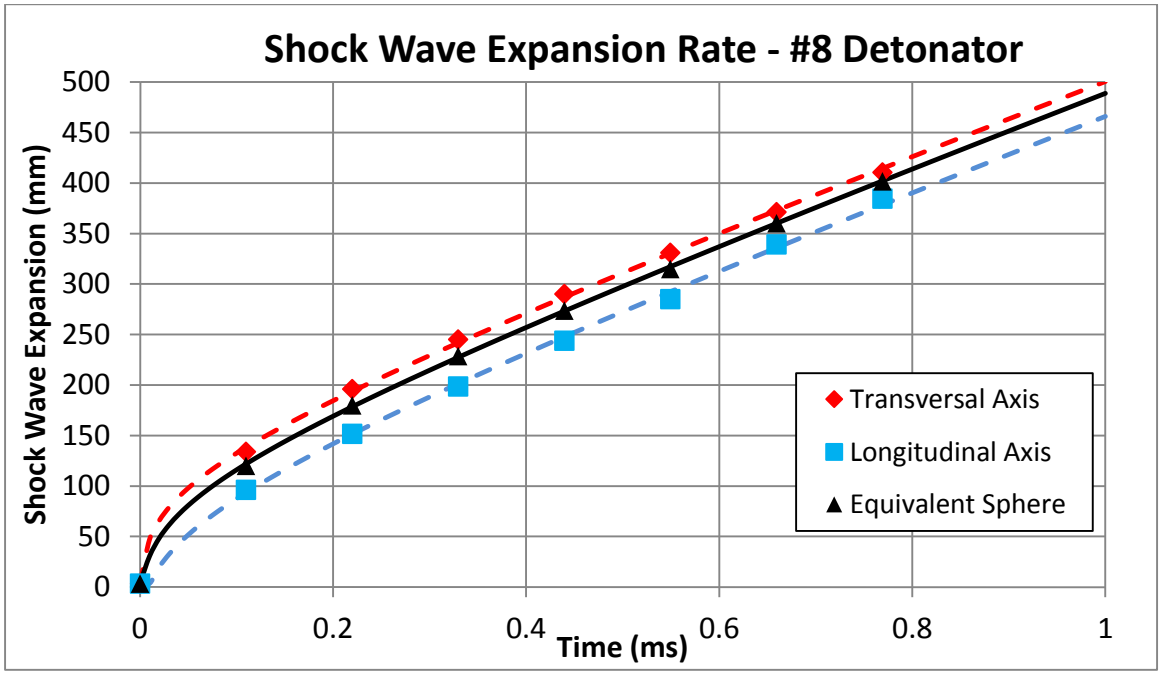

Figure 10. Shock wave expansion rate for number #8 electric detonator

Although an empirical correlation, Equation 1 does satisfy the appropriate physical condition as the time tends to infinity, ensuring that the shock wave velocity approaches the atmospheric speed of the sound [16]. Next, by simply deriving Equation 1, an expression for the shock velocity versus time is obtained. From there, Mach number versus time can be determined, and consequently the blast incident overpressure by using Equation 3. The following figures represent the value of the peak incident

overpressure versus distance from the center of the explosion in logarithmic scale for detonators number 6 and 8. Such graphs can be used for the calculation of the explosive yield. In addition, Edgerton shadowgraph allows calculating the blast in a specific direction from the charge.

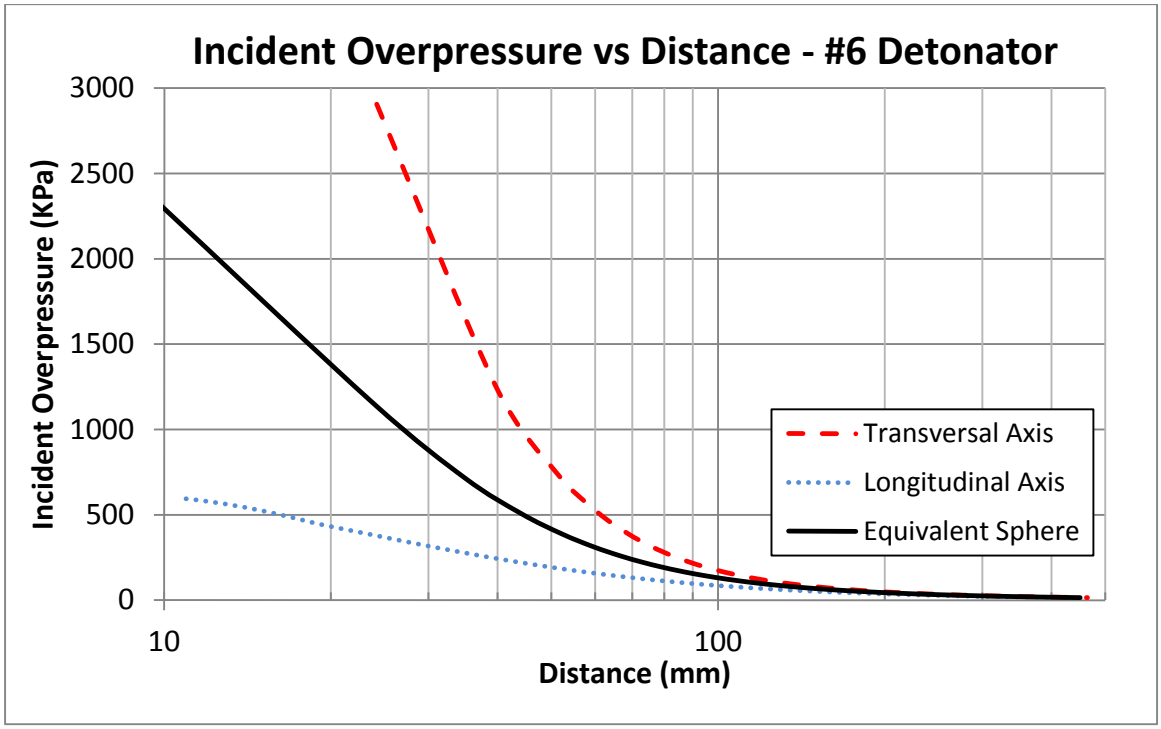

Figure 11. Incident Overpressure vs Distance for number #6 electric detonator

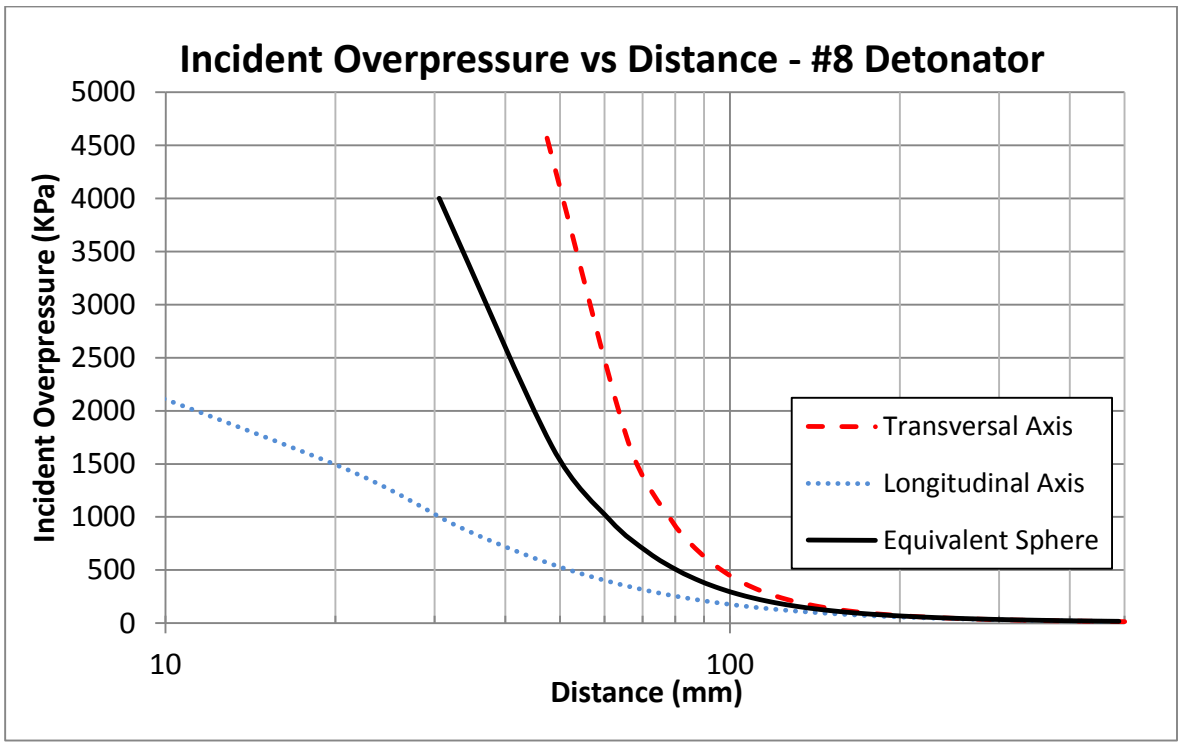

Figure 12. Incident Overpressure vs Distance for number #8 electric detonator

In order to validate the level of accuracy provided by the Edgerton shadowgraph method for detonator characterization, the values of overpressure recorded by optical techniques and from the pressure gauges are compared. This information is summarized in the following table where the percent difference between each pair of values is calculated:

Table III. Blast overpressure gauge readings and values calculated from shadowgraph

Detonator	Direction	Gauge Reading	Shadowgraph	%Difference
#8	Gauge A	28.88 KPa	28.84 KPa	0.14%
	Gauge B	26.42 KPa	26.26 KPa	0.61%
#6	Gauge A	13.08 KPa	16.63 KPa	23.89%
	Gauge B	16.54 KPa	15.70 KPa	5.21%

Table III shows good correlation between the experimental pressure recorded from the retro-reflective shadowgraph and the pressure gauges. Pressure A recorded an unusual low value of blast overpressure during the experiment with the detonator number #6. One possible explanation is the error in the pencil orientation producing a lower value than expected because of the oblique shock interaction.

By comparing the values of peak incident overpressure calculated at different distance from each detonator, one can estimate the percent difference between number 6 and number 8 detonators. The next table shows a summary of the peak incident overpressure generated by each detonator at 200 mm and 400 mm from the center of the explosion and for each axis.

Table IV. Blast overpressure comparison for detonators number 6 and number 8

Distance	Direction	#6 Detonator	#8 Detonator	%Difference
200 mm	Transversal	47.80 KPa	72.02 KPa	**40.43%**
	Longitudinal	36.63 KPa	59.65 KPa	**47.81%**
400 mm	Transversal	17.33 KPa	20.98 KPa	**19.06%**
	Longitudinal	16.21 KPa	22.86 KPa	**34.04%**

Finally, the positive phase duration is measured and an approximation of the energy fluence from the detonator to the ambient air is performed. Calculation of the positive phase duration from the shock Mach number versus distance was initially proposed by Kinney and Graham (1985) and successfully reported by other researchers [15, 16, and 19]. From the instant value of the blast incident overpressure, the positive time duration, and the acoustic impedance of the air, a value of the energy (KJ) per unit area (m^2) can be obtained for different distances from the detonator by using the simplified expression in Equation (4). The results obtained for Number 6 and Number 8 electric detonators are presented in the following graphs with horizontal and vertical logarithmic scales:

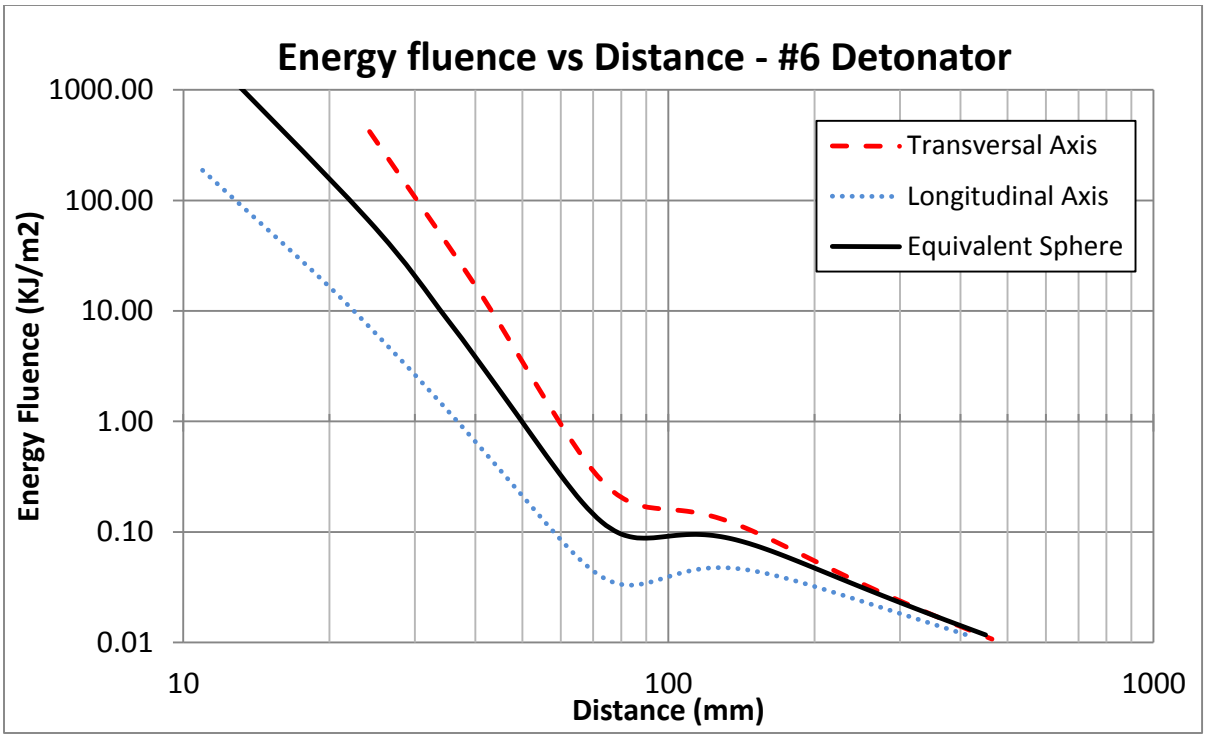

Figure 13. Energy fluence vs distance in air for electric #6 detonator

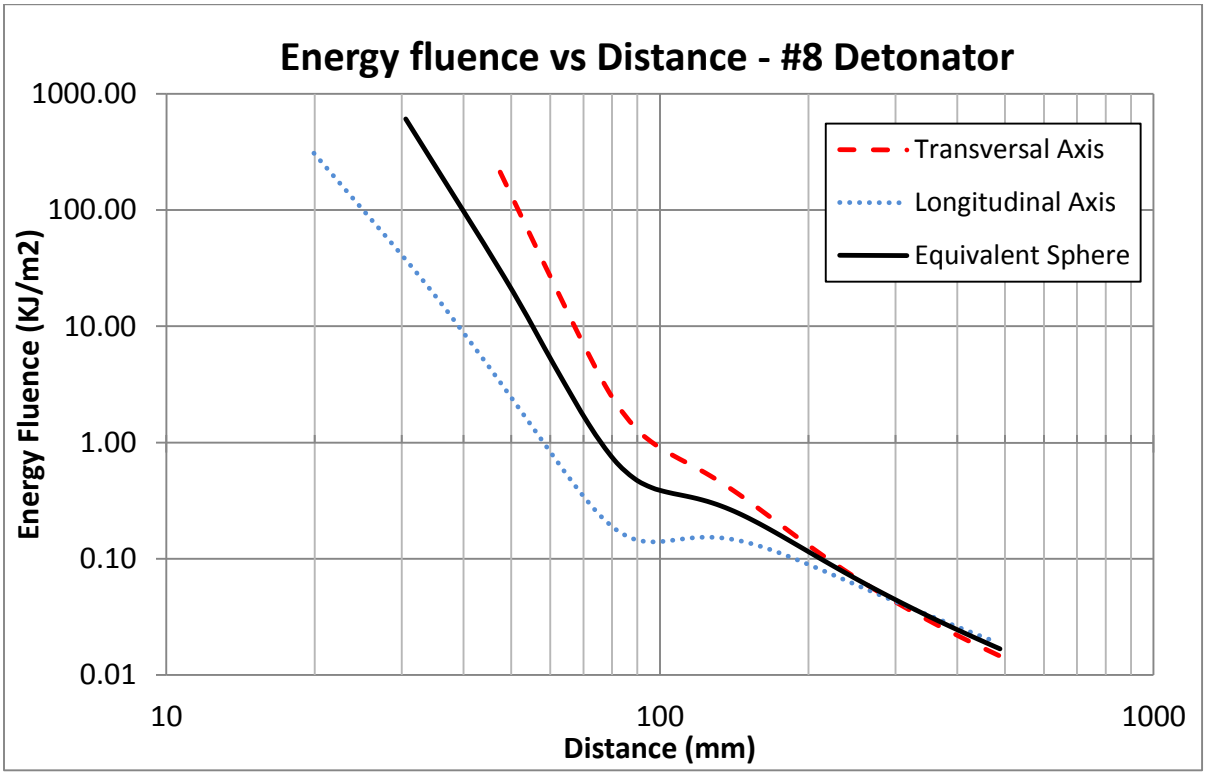

Figure 14. Energy fluence vs distance in air for electric #8 detonator

As shown in Figures 13 and 14, the energy fluence has a decreasing tendency with the distance for both detonators. Even though, the duration of the positive shock increases with the distance from the

explosion as it propagates through a medium, the energy fluence is also function of the square pressure which decays exponentially. Higher values of energy fluence are also observed for the number 8 detonator due to a higher net explosive content. For both experiments, the value of the acoustic impedance was obtained from the air density (1.2 kg/m^3) and the speed of sound (343.21 m/s).

Each high explosive was found to have a unique range of energy fluence above which prompt detonation was always obtained, and below it was not. The average of this range is called the "critical energy fluence" and it represents the amount of energy per unit area (KJ/m2) that the explosive needs in order to be initiated by shock. Reference values for different types of explosives material can be found in the literature [10]. The characterization of a detonator is based on its ability as initiation system and therefore a measure of the shock energy per unit area seems appropriate. For the purpose of this paper, only the energy from the chemical reaction is accounted. Primary fragmentation from the casing also carries a certain amount of kinetic energy that may take part in the initiation of a firing sequence. Additionally, it must be recalled that the term energy fluence is a measure of the energy transferred and therefore it is dependent not only on the energy source but also on the material o medium receiver. This receiver is characterized by its acoustic impedance. Therefore by the use of the Hugoniot curves for both, initiator and acceptor; the amount of energy transferred can be predicted. Future work should aim to the characterization of such detonators in alternative mediums.

6. Conclusion

The retro-reflective shadowgraph technique for measuring shock from high explosives has proven to be a fast and accurate tool for charactering the strength of detonators and blast waves in general. This paper provides a full description of the methodology for and validation for the study of explosive energy from standard Number 6 and Number 8 detonators. By measuring the shock wave expansion rate from each initiation system, a complete characterization of the blast is performed with a high level of accuracy. Shock wave velocity, incident shock Mach number, peak incident overpressure, and time duration are successfully calculated versus distance and time scales. Optical measurements are additionally validated with piezoelectric pressure gauges that recorded overpressure vs time histories at specific locations.

Because of their geometry, standard detonators show an initial ellipsoidal shock expansion that degenerates in a final spherical wave. This non-uniform shape of the shock derives in different blast overpressure values in the different directions. For this reason, transversal and longitudinal directions from the body detonator are studied along with an equivalent spherical blast for convenience purposes. Finally, an approximation of the energy fluence from each detonator in ambient air is performed. The results can be extrapolated to other fluids and materials by using the Hugoniot curves and therefore the shock initiation performance of each detonator can be established under different conditions.

Acknowledgements

We would like to thank the Colorado School of Mines Mining Engineering Department for the use of explosive research laboratory. We would also like to thank Jonathan Mace, from Los Alamos National Laboratory, for providing us with the knowledge and equipment to develop our shadowgraphy research capabilities. As well, we would like to acknowledge the support of Vision Research, specifically Frank Mazella and Rick Robinson, for their support and encouragement for the advancement of our experimentation.

References

[1] Edgerton, H. E., "Shockwave photography of large subjects in daylight" Review of Scientific Instruments 29 2:171-172 (1958)

[2] Settles,G.S.,T.P.Grumstrup,J.D.Miller,M.J.Hargather,L.J.Dodson,andJ.A.Gatto, "Full-scale high-speed 'Edgerton' retro-reflective shadowgraphy of explosions and gunshots," Proc. 5th Pacific Symp. on Flow Visualisation and Image Processing, PSFVIP5, paper 251 (Australia, 27-29 September 2005)

[3] Biele, J. K., "Point-source spark shadowgraphy at the historic birthplace of supersonic transportation - A historical note," Shock Waves 13 3:167-177 (2003)

[4] Parthasarathy S. P., Y. I. Cho, and L. H. Back, "Wide-field shadowgraphy of tip vortices from a helicopter rotor," AIAA Journal 25 1:64-70 (1987)

[5] Settles, G. S, "High-speed imaging of shock waves, explosions and gunshots," American Scientist 94 1:22-31 (2006)

[6] Hargather, M. J., G. S. Settles, J. A. Gatto, T. P. Grumstrup, and J. D.Miller, "Full-scale optical experiments on the explosive failure of a ULD-3 air cargo container," Proc. 4th International Aviation Security Technology Symp., (Washington DC, Nov. 2006)

[7] Virtual Backgrounds, 101 Uhland Road, Ste. 106, San Marcos, TX 78666 (USA), 1-800- 831-0474, www.virtualbackgrounds.net

[8] Hargather, M. J., G. S. Settles, and J. A. Gatto, "Gram-range explosive blast scaling and associated materials response," Proc. ISSW26, paper 3131 (July 2007)

[9] G.S. Settles "Schlieren and Shadowgraph Techniques: Visualizing Phenomena in Transparent Media" ISBN 978-3-642-63034-7, Springer-Verlag Berlin Heidelberg 2001.

[10] P.W. Cooper, "Explosives Engineering", ISBN 0-471-18636-8, 1966.

[11] W.E.Deal, "Shock Hugoniot of Air", Journal of Applied Physics, 1957.

[12] M.M.Biss, "Energetic Material Detonation Characterization: A laboratory –scale Approach", Propellants, explosives, and pyrotechnics, 38, 477-485, 2013.

[13] E.D. Esparza, "Spherical Equivalency of Cylindrical Charges in Free-Air", Southwest Research Institute, 25th Department of Defense Explosives Safety Seminar, 1992.

[14] J. M. Dewey, Air velocity in blast waves from TNT explosions, Royal Society of London Proceedings Series A 1964, 279, 366-385.

[15] M. J. Hargather, "Scaling, characterization, and application of gram-range explosive charges to blast testing of materials", Pennsylvania State University, 2008

[16] M.M.Biss, “Characterization of blast from labotaroy-scale composite explosive charges”, Pennsylvania State University, 2008

[17] G.F. Kinney, K.J.Graham, “Explosive Shocks in Air”, Second Edition, 1985.

[18] M. J. Hargather and G. S. Settles, Optical measurement and scaling of blasts from gram-range explosive charges, Shock Waves 2007, 17, 215-223.

[19] G. I. Taylor. The formation of a blast wave by a very intense explosion .1. Theoretical discussion. *Proceedings of the Royal Society of London Series A-Mathematical and Physical Sciences*, 201(1065):159–174, 1950.